Travelling waves in a radiation-combustion free-boundary model for flame propagation

Jan Bouwe van den Berg, Hala Elrofai and Josephus Hulshof
Department of Mathematics, VU University Amsterdam,
De Boelelaan 1081, 1081 HV Amsterdam, The Netherlands,
janbouwe@few.vu.nl, elrofai@few.vu.nl, jhulshof@few.vu.nl

February 12, 2008

Abstract

We study a combustion-radiation model which models premixed flames propagating in a gaseous mixture with inert dust. This model combines diffusion of mass and temperature with reaction at the flame front. We choose a free boundary model to describe the propagating flames and take a linearised approximation to model the radiation, but we keep a nonlinear reaction term which is temperature dependent. The radiative transfer of thermal energy emitted and absorbed by dust is modelled using the Eddington equation. We analyse the bifurcation diagram of the travelling wave solution curve. In a specific parameter plane, travelling waves are given by a single smooth curve which is parameterised by the flame temperature.

1 Introduction

Combustion has a wide variety of applications, but also appears naturally in less controlled situations such as forest fires and tunnel accidents. The different physical and chemical aspects of combustion have been modelled extensively in the past, e.g. [9]. The resulting models are often complicated and difficult to analyse mathematically. Our goal in this paper is to study a combustion-radiation model that incorporates the relevant physical aspects, but is simple enough from a mathematical point of view to be investigated analytically. We therefore choose a free boundary model to describe the propagating flame and we take a linearised approximation to model the radiation, but we keep a nonlinear reaction term. This model describes flames in gaseous mixtures in which thermal radiation due to the presence of dust enhances the reaction. It is based on the hypotheses of simple chemistry and high activation energy, and was suggested first by Buckmaster and Joulin [3, 4, 6].

Without radiative effects the model is known as the thermo-diffusive model for premixed flames, also referred to as the adiabatic case. The reaction is assumed to be confined to an infinitesimally

narrow reaction zone (the flame front), which separates the fresh region in front of the flame from the burnt region behind the flame, in which the mass fraction is assumed to be identically zero, see Figure 1. At the flame front the mass flux going into the flame balances the heat flux coming out of the flame, with a temperature dependent Arrhenius type reaction rate. In this model planar flames are

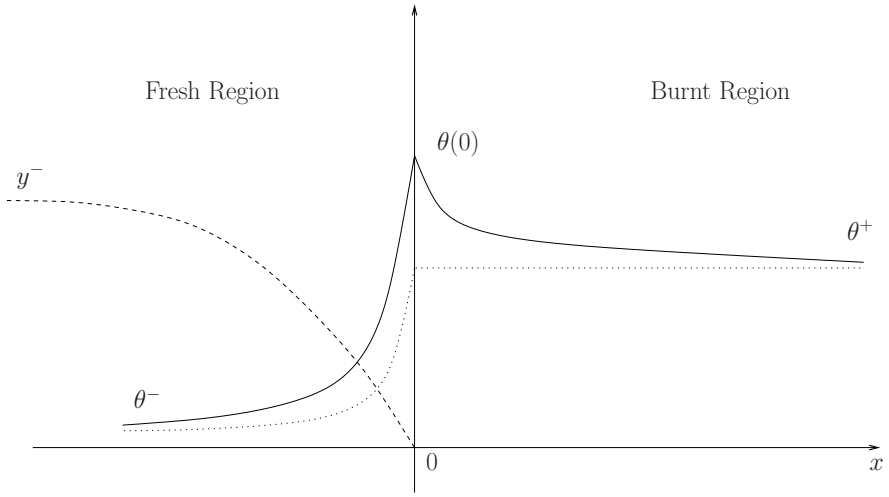

Figure 1: Typical temperature profiles for the fuel (dashed line) and for the temperature (solid and dotted lines). The dotted line depicts the adiabatic case (no radiation), while the solid line represents the full problem, including radiative effects. Note that the flame temperature is higher in the latter case.

one-dimensional travelling wave solutions characterised by the amount of fuel y^- in the fresh region far ahead of the flame front, and the temperatures θ^- and θ^+ far ahead and far behind of the flame front. For travelling waves, a global conservation law implies that

$$\theta^+ = y^- + \theta^-. \tag{1.1}$$

Note that y^-, which we think of as the amount of fuel fed to the flame, is a natural control or bifurcation parameter. Fixing θ^- we may (and will) however just as well use θ^+ for this purpose on the horizontal axis in the bifurcation diagrams. On the vertical axis the flame itself will be characterised by its flame speed μ. The flame temperature is less suited for this purpose. However, it will appear in due course as the natural parameter along the solution curve in the bifurcation diagram, which, unless stated otherwise, is the first quadrant in the (θ^+, μ)-plane.

In the absence of radiation, the travelling waves are given by explicit exponential functions in the fresh region. Behind the flame, in the burnt region, the temperature is identically equal to θ^+ and coincides with the flame temperature θ^*. The flame speed μ is related to the reaction rate $F = F(\theta^*)$ by

$$\mu = \frac{F(\theta^*)}{\theta^+ - \theta^-}, \tag{1.2}$$

so in the adiabatic case the solution curve in the bifurcation diagram is given by setting $\theta^* = \theta^+$ in this formula.

The radiative transfer of thermal energy emitted and absorbed by dust particles is modelled using the Eddington approximation for the radiation field. Radiative transfer may significantly influence the flame speed and the temperature profile, depending on the opacity of the medium. A general feature is the Joulin effect: due to the radiative effects the flame temperature is higher than the adiabatic temperature (see Figure 1) and the flame propagates with a larger speed.

With the radiative effects included in the model, there are still travelling wave solutions, but no longer in closed form, see [2], where existence of such solutions was proved, and [1], where in a limit case nontrivial bifurcation diagrams with turning points and changes of stability where obtained.

The full radiative model studied in this paper, see e.g. [2, 3], consists of a system of two linear diffusion equations for the fuel mass fraction $Y(x,t)$ and the temperature $\Theta(x,t)$, which are coupled to the Eddington equation for the radiative flux $Q(x,t)$, all as functions of position x and time t. Representing the infinitesimally thin sheet where the reaction occurs (the flame front) by the free boundary $x = s(t)$, the equations in non-dimensional form are then written in one spatial dimension as

$$Y_t = \frac{1}{\mathrm{Le}} Y_{xx} \qquad x < s(t), \tag{1.3}$$

$$\Theta_t = \Theta_{xx} - \beta Q_x \qquad x \neq s(t), \tag{1.4}$$

$$-Q_{xx} + 3\alpha^2 Q = -\alpha \left(\Theta^n\right)_x \qquad x \neq s(t). \tag{1.5}$$

The equation (1.3) for Y contains the Lewis number, the ratio between the diffusivities of Θ and Y. Note that fuel is absent in the burnt region, i.e. $Y(x,t) = 0$ for $x \geq s(t)$. Besides the divergence of the thermal flux, (1.4) contains the divergence of the radiative flux, which appears with a coefficient β, called the Boltzmann number. The Boltzmann number is a measure for the ratio between the effect of radiative and thermal convection. The equation for the radiative flux contains two parameters, n, to be discussed shortly, and α, the opacity, which is related to the inverse of the mean free path length of a photon.

The jump conditions at the free boundary between the fresh region and the burnt region are

$$Y = [\Theta] = 0; \qquad \frac{1}{\mathrm{Le}} Y_x = [\Theta_x] = -F(\Theta); \qquad [Q] = [Q_x] = 0. \tag{1.6}$$

Here the square brackets denote the jumps at $x = s(t)$ and $F(\Theta)$ is the reaction rate. The jump conditions for Y and Θ state that the reaction rate $F(\Theta)$ is equal to the fuel flux going into the flame, which in turn balances the heat flux coming out of the flame. Note that the zero jump conditions for Q and Q_x are equivalent to posing (1.5) on the whole line in a distributional sense.

In [2] it was shown that there exist travelling wave solutions under the condition that the reaction rate $F(\Theta)$ is a bounded positive increasing continuous function of temperature, such as the Arrhenius law taken in this paper,

$$F(\theta^*) = \exp\left(\frac{1}{\varepsilon}\left(\frac{1}{\theta_c} - \frac{1}{\theta^*}\right)\right), \tag{1.7}$$

in which ε is the reciprocal of the activation energy, θ^* is the flame temperature, and θ_c is a suitable characteristic temperature. The existence result holds for all positive value of the parameters y^-, θ^-, Le, α and β, but it gives no information on the multiplicity of solutions.

In the physical model the radiation is modeled by black body radiation, corresponding to $n = 4$. In this paper we study the "linear" problem $n = 1$. We consider this linearised problem for two main reasons. Firstly the nonlinearity can be approximated by the linearisation around a "typical" temperature Θ_0 (cf. [7]),

$$\Theta^4 \approx \Theta_0^4 + 4\Theta_0^3(\Theta - \Theta_0), \tag{1.8}$$

and then by taking the position derivative of (1.8) and rescaling Q and β by $Q = 4\Theta_0^3\hat{Q}$ and $\beta Q = \hat{\beta}\hat{Q}$, we obtain (1.5) with $n = 1$. Secondly, the problem is much easier to treat from a mathematical point of view. Note though that the "linear" problem is still strongly nonlinear due to the position of the free boundary being unknown a priori, as well as the reaction rate $F(\Theta)$ being nonlinear. Because the simplified problem keeps this feature of nonlinearity, it turns out that the information we obtain for $n = 1$ gives insight in the physical case $n = 4$.

In Section 2 we describe the travelling wave problem and derive an expression

$$\theta^* = \theta^+ + (\theta^+ - \theta^-)g(\mu) \tag{1.9}$$

for the flame temperature for a prescribed flame speed μ, in the case that the reaction rate is not specified.

In section 3 we specify the reaction rate as a smooth positive increasing function of the flame temperature θ^*, derive (1.2) and combine it with (1.9) to describe the (θ^+, μ)-bifurcation diagram. The travelling wave solutions are given by *a single smooth curve parameterised by the flame temperature* θ^*. We discuss this solution curve and show that it may exhibit $S-$shaped parts and turning points, see Figure 2.

Numerical computations are performed in Section 4, combining the obtained expression for θ^* with the reaction rate, to plot bifurcation diagrams for μ versus θ^+ for various values of the parameters.

In Section 5 we examine some natural asymptotic limit cases of the radiative parameters α and β. We compare the obtained expressions to those obtained in [2] and derive a formula for the speed law in the asymptotic regime in which the Joulin effect is most pronounced: $\alpha \to 0$, $\beta \to \infty$ and $\alpha\beta \to 0$. Here this asymptotic regime has to be coupled to that of small ε (large activation energy). The analytically obtained asymptotic speed law is analogous to the one derived formally in [8] for the nonlinear problem.

2 The travelling wave system

We denote the travelling wave variable by $\tilde{x} = x + \mu t$. In a comoving frame the equations are obtained by substituting $s(t) = \tilde{s}(t) - \mu t$, $Y(x,t) = \tilde{Y}(\tilde{x},t)$, $\Theta(x,t) = \tilde{\Theta}(\tilde{x},t)$ and $\beta Q(x,t) = \tilde{Q}(\tilde{x},t)$ in (1.3),

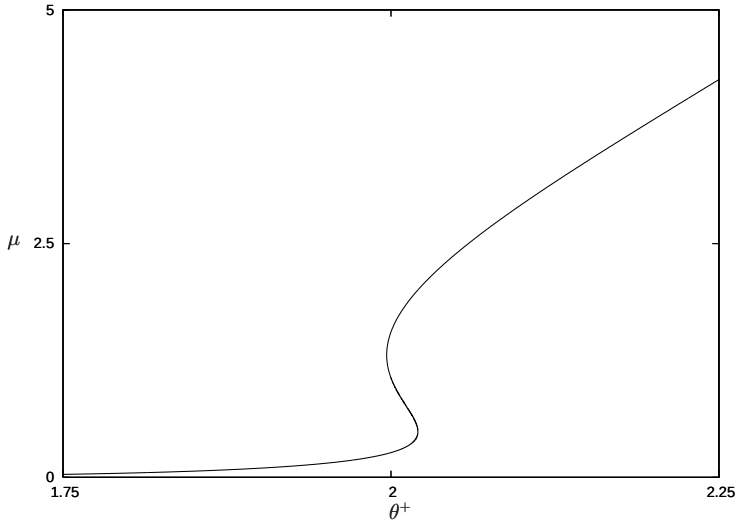

Figure 2: The solution diagram in the (θ^+,μ)-plane parameterised by θ^*.

(1.4) and (1.5). Dropping the tildes we obtain

$$Y_t = \frac{1}{\mathrm{Le}} Y_{xx} - \mu Y_x \qquad x < s(t), \tag{2.1}$$

$$\Theta_t = \Theta_{xx} - \mu \Theta_x - Q_x \qquad x \neq s(t), \tag{2.2}$$

$$-Q_{xx} + 3\alpha^2 Q = -\alpha\beta(\Theta^n)_x \qquad x \neq s(t). \tag{2.3}$$

Note that we have scaled Q to move the radiative parameter β to the equation for the radiative flux. The jump conditions are again given by (1.6).

2.1 Travelling waves

Travelling wave solutions correspond to stationary solutions of the problem in comoving variables and are denoted by the corresponding lower case variables y, θ, q.

Introducing $\alpha\beta = \chi$ as a new parameter and fixing the stationary free boundary at the origin, the travelling wave problem becomes

$$\mu y' = \frac{1}{\mathrm{Le}} y'' \qquad x < 0, \tag{2.4}$$

$$\mu \theta' = \theta'' - q' \qquad x \neq 0, \tag{2.5}$$

$$-q'' + 3\alpha^2 q = -\chi(\theta^n)' \qquad x \neq 0, \tag{2.6}$$

with jump conditions in $x = 0$ given by

$$y(0) = [\theta] = 0; \qquad -\frac{1}{\mathrm{Le}} y'(0) = -[\theta'] = F(\theta(0)); \qquad [q] = [q'] = 0. \tag{2.7}$$

The limiting values at $\pm\infty$ are denoted by

$$y(-\infty) = y^-; \quad \theta(\pm\infty) = \theta^\pm.$$

In view of these limiting values, travelling wave solutions move to the left (into the fresh region) along the x axis with flame speed $\mu > 0$.

The governing equation (2.4) for the fuel mass fraction decouples and gives

$$y(x) = y^-(1 - \exp(\mu \mathrm{Le} x)). \tag{2.8}$$

Thus it only remains to solve (2.5) and (2.6) with jump conditions (2.7). Integrating (2.5) over the whole line gives

$$\mu(\theta^+ - \theta^-) = -[\theta'] = F(\theta^*). \tag{2.9}$$

Combining (2.9) with (2.8) and the jump condition in (2.7), we obtain the global conservation law

$$\theta^+ = \theta^- + y^-. \tag{2.10}$$

With $n = 1$ the "linear" equations, which read

$$\mu\theta' = \theta'' - q' \qquad x \neq 0, \tag{2.11}$$

$$-q'' + 3\alpha^2 q = -\chi\theta' \qquad x \neq 0, \tag{2.12}$$

can be solved in terms of θ' and q as linear combinations of

$$\begin{pmatrix} \theta' \\ q \end{pmatrix} = \begin{pmatrix} A \\ B \end{pmatrix} \exp(ax). \tag{2.13}$$

For A, B and a we find

$$(\mu - a)A + aB = 0, \tag{2.14}$$

$$\chi A + (-a^2 + 3\alpha^2)B = 0. \tag{2.15}$$

Equations (2.14) and (2.15) have a nontrivial solution if and only if a is a root of the third order polynomial (c.f. [3])

$$P(a) = (a^2 - 3\alpha^2)(a - \mu) - \chi a. \tag{2.16}$$

Considering the two terms of $P(a)$ separately, i.e. $P_1(a) = (a^2 - 3\alpha^2)(a - \mu)$ and $P_2(a) = a\chi$, we see that, as illustrated in Figure 3, $P_1(a)$ and $P_2(a)$ have three intersections, two with $a > 0$ and one with $a < 0$ (recalling that μ, α and χ are positive). We denote the positive roots of $P(a)$ by $a_1 > a_2$, and the negative root by a_3.

Both θ' and q should vanish at infinity, thus we must choose the positive roots for $x < 0$ where, using (2.14), we have

$$\theta_l' = A_1 \exp(a_1 x) + A_2 \exp(a_2 x), \tag{2.17}$$

$$q_l = -\frac{A_1(\mu - a_1)}{a_1} \exp(a_1 x) - \frac{A_2(\mu - a_2)}{a_2} \exp(a_2 x), \tag{2.18}$$

while for $x > 0$

$$\theta_r' = A_3 \exp(a_3 x), \tag{2.19}$$

$$q_r = -\frac{A_3(\mu - a_3)}{a_3} \exp(a_3 x). \tag{2.20}$$

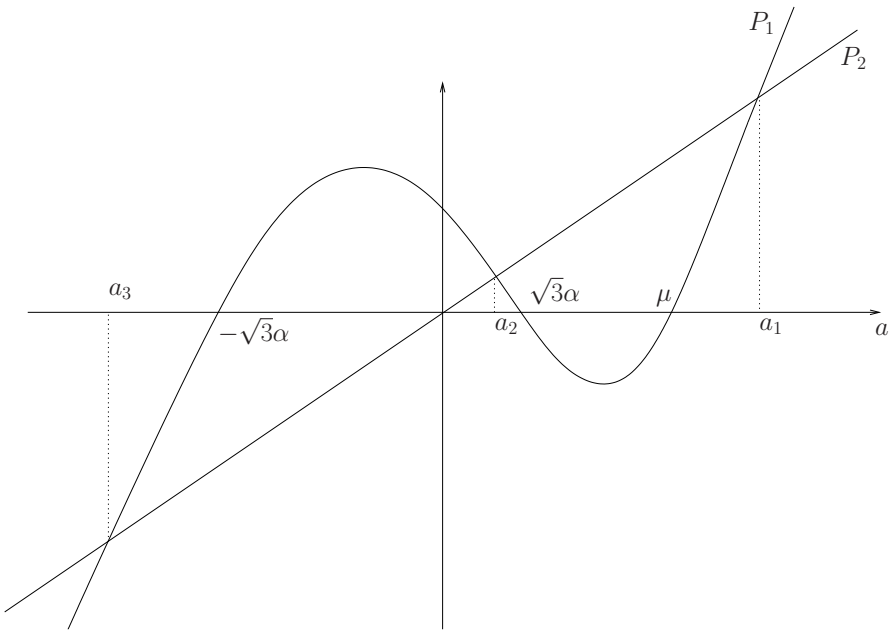

Figure 3: Plot of $P_1(a)$ and $P_2(a)$. In the picture we chose $\mu > \sqrt{3}\alpha$, but this is not relevant for the analysis.

The subscript l and r stand for, respectively, left and right side of the origin. Now using the above formulas (2.18) and (2.20) for q, we obtain from the zero jump conditions for q and q' in (2.7) that

$$\frac{A_1(\mu - a_1)}{a_1} + \frac{A_2(\mu - a_2)}{a_2} - \frac{A_3(\mu - a_3)}{a_3} = 0, \tag{2.21}$$

$$A_1(\mu - a_1) + A_2(\mu - a_2) - A_3(\mu - a_3) = 0. \tag{2.22}$$

By solving (2.21) and (2.22), we find A_1 and A_2 as functions of A_3:

$$A_1 = -\frac{a_1 A_3(\mu - a_3)(a_2 - a_3)}{a_3(a_1 - a_2)(\mu - a_1)}, \tag{2.23}$$

$$A_2 = \frac{a_2 A_3(\mu - a_3)(a_1 - a_3)}{a_3(a_1 - a_2)(\mu - a_2)}. \tag{2.24}$$

A glance at Equation (2.16) and Figure 3 shows that $a_2 < \mu < a_1$ and $a_3 < -\sqrt{3}\alpha$, and therefore the denominators of (2.23) and (2.24) are never equal to zero. We use these expression for A_1 and A_2 to express θ_l' and θ_r' in terms of A_3. After integrating we obtain, using $\theta_l = \theta_r$ at $x = 0$, that

$$\theta_l = \theta^- + (\theta^+ - \theta^-)\frac{\mu - a_3}{a_1 - a_2}\left(\frac{\mu - a_2}{a_1 - a_3}e^{a_1 x} + \frac{a_1 - \mu}{a_2 - a_3}e^{a_2 x}\right), \tag{2.25}$$

$$\theta_r = \theta^+ + (\theta^+ - \theta^-)\frac{(a_1 - \mu)(\mu - a_2)}{(a_1 - a_3)(a_2 - a_3)}e^{a_3 x}. \tag{2.26}$$

Note that all the coefficients are positive. The flame temperature $\theta^* = \theta(0)$ can be obtained either

from (2.25) or (2.26) by putting $x = 0$,

$$\theta^* = \theta^+ + \frac{(\theta^+ - \theta^-)(a_1 - \mu)(\mu - a_2)}{(a_1 - a_3)(a_2 - a_3)}. \tag{2.27}$$

Thus we have established:

Proposition 2.1 *If we drop the reaction rate F from the (jump) conditions (2.7), there exists a travelling wave profile for every value of the flame speed $\mu > 0$, The flame temperature is given by*

$$\theta^* = \theta^+ + (\theta^+ - \theta^-)g(\mu), \tag{2.28}$$

where

$$g(\mu) = \frac{(a_1 - \mu)(\mu - a_2)}{(a_1 - a_3)(a_2 - a_3)} = \frac{P(\mu)}{P'(a_3)(a_3 - \mu)} = \frac{\mu\chi}{P'(a_3)(\mu - a_3)} > 0, \tag{2.29}$$

and $a_3 < 0 < a_2 < \mu < a_1$ are the roots of the cubic P defined in (2.16).

Clearly $g(\mu)$ is a smooth function of $\mu \in [0, \infty)$ with $g(0) = 0$. The positivity of $g(\mu)$ for $\mu > 0$ follows since $P'(a_3) > 0$ in view of the ordering $a_3 < 0 < a_2 < \mu < a_1$. Rewriting $P(a) = 0$ as

$$a - \mu = \frac{\chi a}{a^2 - 3\alpha^2},$$

we see that as $\mu \to \infty$

$$a_1 - \mu \sim \frac{\chi}{a_1} \sim \frac{\chi}{\mu}; \quad a_{2,3} \to \pm\alpha\sqrt{3}; \quad g(\mu) \sim \frac{\chi}{2\alpha\sqrt{3}\mu},$$

whence $g(\infty) = 0$. Next we show that $g(\mu) < 1$ for all $\mu > 0$, in agreement with the a priori upper bound $\theta^+ + y^- = 2\theta^+ - \theta^-$ for θ conjectured by Joulin and established in [2].

Arguing by contradiction, assume $g(\mu) = 1$ for some $\mu > 0$. In view of (2.29) it follows that

$$(a_3 - \mu)P'(a_3) + \mu\chi = 0, \tag{2.30}$$

another cubic equation for a_3. By (2.16)

$$a_3^3 = \mu a_3^2 + (3\alpha^2 + \chi)a_3 - 3\alpha^2\mu.$$

Substituting this in (2.30) we obtain that the quadratic polynomial

$$\mu a_3^2 - (3\alpha^2 + \chi + \mu^2)a_3 + \mu(3\alpha^2 - \chi)$$

must be zero. Multiplying the latter polynomial by a_3 and subtracting $0 = \mu P(a_3)$ we obtain that

$$(3\alpha^2 + \chi)a_3^2 - 6\mu\alpha^2 a_3 + 3\alpha^2\mu^2 = 0,$$

a contradiction because $a_3 < 0$. This means that $g(\mu)$ is never equal to 1.

The above reasoning establishes

Proposition 2.2 *The function g defined by (2.29) is a smooth function of $\mu \in [0,\infty)$ with $g(0) = g(\infty) = 0$ and $0 < g(\mu) < 1$ for all $\mu > 0$. Moreover $g(\mu)$ has a unique extremal value (a positive maximum) on $[0,\infty)$ at*

$$\mu = \left(\frac{(3\alpha^2+\chi)^3}{3\alpha^2}\right)^{\frac{1}{4}}. \tag{2.31}$$

This critical value of μ follows from the fact that $g'(\mu)$ has only one zero at (2.31) as we will show below. From (2.29) we have

$$\begin{aligned}\frac{g'(\mu)}{\chi} &= \frac{1}{P'(a_3)(\mu-a_3)} + \mu\frac{d}{d\mu}\left(\frac{1}{P'(a_3)(\mu-a_3)}\right)\\ &= \frac{1}{P'(a_3)(\mu-a_3)} - \frac{\mu[(1-a_3')P'(a_3)+(\mu-a_3)(P''(a_3)a_3'+P_\mu'(a_3))]}{[P'(a_3)(\mu-a_3)]^2}.\end{aligned} \tag{2.32}$$

where $a_3' = \frac{da_3}{d\mu}$, $P' = \frac{\partial P}{\partial a}$, $P_\mu = \frac{\partial P}{\partial \mu}$ and $P_\mu' = \frac{\partial^2 P}{\partial\mu\partial a}$.

The first term of (2.32) is simple. We denote the coefficient of μ in the numerator of the second term by

$$\gamma = (1-a_3')P'(a_3) + (\mu-a_3)(P''(a_3)a_3' + P_\mu'(a_3)) \tag{2.33}$$

We need an expression for a_3' and we find it by differentiating $P(a_3,\mu)$ with respect to μ. This gives

$$0 = \frac{\partial P}{\partial a_3}a_3' + \frac{\partial P}{\partial \mu},$$

whence

$$a_3' = \frac{a_3^2 - 3\alpha^2}{P'(a_3)}. \tag{2.34}$$

Substituting (2.34) in (2.33) and using (2.16) to simplify the result we obtain

$$\gamma = \frac{24\alpha^2(a_3-\mu)^2 + \chi(\chi+3\alpha^2-a_3^2)}{P'(a_3)} = \frac{\tilde\gamma}{P'(a_3)} > 0. \tag{2.35}$$

In section 3 we will use the inequality (2.35). The sign of the denominator of (2.35) is positive. The first term of numerator is obviously positive. From the fact that $P(-\sqrt{3\alpha^2+\chi}) = -\mu\chi < 0$ it follows that $a_3 > -\sqrt{3\alpha^2+\chi}$. This implies that the second term in the numerator is also positive so that $\gamma > 0$.

Substituting (2.35) in (2.32) we obtain, by using $P(a_3) = 0$,

$$\begin{aligned}\frac{g'(\mu)}{\chi} &= \frac{(P'(a_3))^2(\mu-a_3) - \mu\tilde\gamma}{(P'(a_3))^3(\mu-a_3^2)^2}\\ &= \frac{-4(((3\alpha^2+\chi)^2 - 3\alpha^2\mu^2)a_3 - 3\alpha^2\mu(3\alpha^2+\chi-\mu^2))}{(P'(a_3))^3(\mu-a_3^2)^2}.\end{aligned}$$

Thus for $g'(\mu)$ to be zero, a_3 has to satisfy

$$a_3 = \frac{3\alpha^2\mu(3\alpha^2+\chi-\mu^2)}{(3\alpha^2+\chi)^2 - 3\alpha^2\mu^2}$$

and, by using $P(a_3) = 0$, the latter is equivalent to $(3\alpha^2+\chi)^3 - 3\alpha^2\mu^4 = 0$, whence (2.31) follows.

3 Traveling wave solution curve in the bifurcation diagram

In view of (2.28) and (2.9) the travelling wave problem is now equivalent to the algebraic system

$$\theta^+ + (\theta^+ - \theta^-)g(\mu) = \theta^*, \tag{3.1}$$

$$\mu(\theta^+ - \theta^-) = F(\theta^*), \tag{3.2}$$

where $g(\mu)$ is given by (2.29). The determinant of the derivatives of the left hand sides of (3.1,3.2) with respect to θ^+ and μ is

$$(\theta^+ - \theta^-)(1 + g(\mu) - \mu g'(\mu)). \tag{3.3}$$

As we show below, this expression is nonzero. In view of the implicit function theorem, travelling wave solutions are then, at least locally, given as smooth curves in the (θ^+, μ)-plane. In fact we show that there is only one such curve, parameterised by the flame temperature θ^*, which runs from θ_- to ∞.

To determine the sign of the determinant (3.3) we write

$$\begin{aligned} 1 + g(\mu) - \mu g'(\mu) &= 1 + \chi\mu^2 \frac{d}{d\mu}\left(\frac{1}{(a_3 - \mu)P'(a_3)}\right) \\ &= 1 + \chi\mu^2 \frac{(1 - a_3')P'(a_3) + (\mu - a_3)(P''(a_3)a_3' + P_\mu'(a_3))}{[(a_3 - \mu)P'(a_3)]^2}. \end{aligned} \tag{3.4}$$

Using (2.33), we write (3.4) as

$$1 + g(\mu) - \mu g'(\mu) = 1 + \chi\mu^2 \frac{\gamma}{[(a_3 - \mu)P'(a_3)]^2}. \tag{3.5}$$

In the previous section, (2.35), we have proved the positivity of γ. Thus we conclude that the determinant (3.3) is positive and note that we have in fact shown that

$$g(\mu) > \mu g'(\mu). \tag{3.6}$$

Thus θ^+ and μ are locally parameterised by θ^*. In other words, the bifurcation diagram consists of smooth curves. We now show that there can only be one such curve. Indeed, decreasing θ^* along a solution branch, the curve can be continued as long as θ^+ and μ remain bounded. Clearly (3.1) keeps θ^+ bounded (above by θ^*) as $\theta^* \to \theta^-$. In fact we can rewrite (3.1) as

$$(\theta^+ - \theta^-)(1 + g(\mu)) = \theta^* - \theta^-,$$

showing that, as long as θ^* is away from θ^-, so is θ^+. Hence μ remains bounded away from infinity in view of (3.2). Clearly, as $\theta^* \to \theta^-$, (3.1) forces θ^+ to follow θ^* so that $\theta^+ \to \theta^-$ and, in view of (3.2), $\mu \to \infty$. Solving both (3.1) and (3.2) for θ^+ we find

$$\theta^+ = \frac{\theta^* + g(\mu)\theta^-}{1 + g(\mu)} = \theta^- + \frac{F(\theta^*)}{\mu},$$

in which the second equality implies that, given μ sufficiently large, there can only be one θ^* and hence only one solution branch.

Summing up:

Proposition 3.1 *In the (θ^+, μ)-plane travelling waves are given by a single smooth curve which is parameterised by the flame temperature:*

$$(\theta^-, \infty) \ni \theta^* \quad \longrightarrow \quad (\theta^+(\theta^*), \mu(\theta^*)). \tag{3.7}$$

This solution curve lies in the first quadrant and has

$$\lim_{\theta^* \downarrow \theta^-} (\theta^+, \mu) = (\theta^-, \infty); \qquad \lim_{\theta^* \uparrow \infty} (\theta^+, \mu) = (\infty, 0). \tag{3.8}$$

In view of the implicit function theorem argument the solution curve has no selfintersections.

3.1 Turning points

Before we examine the possibilities for turning points of (3.7), we recall that in the adiabatic case this solution curve is given by

$$\mu = \frac{F(\theta^*)}{\theta^* - \theta^-}, \quad \theta^+ = \theta^*.$$

Clearly the "adiabatic" curve has no vertical turning points, but it may have horizontal turning points. In the case of the Arrhenius law (1.7), one has

$$F'(\theta^*) = \frac{F(\theta^*)}{\varepsilon(\theta^*)^2}, \tag{3.9}$$

hence horizontal turning points are given by the solutions of

$$\theta^* - \theta^- = \varepsilon(\theta^*)^2,$$

so that there are at most two of them.

For the general case, recalling (3.6) and applying the implicit function theorem, we obtain

$$(\theta^+)' = \frac{1 - F'g'}{1 + g - \mu g'}, \tag{3.10}$$

$$\mu' = \frac{(1+g)F' - \mu}{(\theta^+ - \theta^-)(1 + g - \mu g')}. \tag{3.11}$$

Note that primes denote differentiation with respect to the independent variable of the function that is being differentiated: θ^+, μ and F are functions of θ^*, but g is a function of μ.

We see from (3.10) and (3.11) that it is the value of $F' = F'(\theta^*)$ that determines in which direction the solution curve moves in the bifurcation diagram as θ^* is varied. This is in agreement with the limit case analysis in [1]. We note that there are two possibilities for turning points: vertical or horizontal. Vertical points are points where

$$(\theta^+)' = 0 \quad \Leftrightarrow \quad F' = \frac{1}{g'} \quad \Leftrightarrow \quad \mu' = \frac{F'}{\theta^+ - \theta^-} \quad \Rightarrow \quad (\theta^+)'' = -\frac{F''g' + F'g''\mu'}{1 + g - \mu g'}. \tag{3.12}$$

Likewise, horizontal points are points where

$$\mu' = 0 \quad \Leftrightarrow \quad F' = \frac{\mu}{1+g} \quad \Leftrightarrow \quad (\theta^+)' = \frac{F'}{\mu} \quad \Rightarrow \quad \mu'' = \frac{F''}{\theta^+ - \theta^-}\frac{1+g}{1 + g - \mu g'}. \tag{3.13}$$

Of course a turning point also requires a sign change of the relevant derivative. The behaviour of the second derivatives will be used later.

From (3.13) and (3.8) we see that, if the solution curve (3.7) has any turning points at all, the first and the last turning point must be horizontal, because by (3.12) in vertical points $\mu' > 0$. Similarly, $(\theta^+)' > 0$ in horizontal points. Without horizontal turning points there are no vertical points either.

Note that the condition for having a horizontal point is that

$$F'(\theta^*) = \frac{\mu}{1+g}, \tag{3.14}$$

and that in view of (3.3) being positive, the right hand side of (3.14) is an increasing function of μ.

The next proposition sums up what we have so far and includes the results of a discussion below concerning the additional information that follows from the convex-concave form of the Arrhenius law reaction rate.

Proposition 3.2 *Consider the curve of the travelling waves, parameterised by θ^*, in the (θ^+, μ) parameter plane. In horizontal (turning) points the solution curve moves to the right with increasing θ^*. In vertical points it moves upwards. If there is any turning points, then the first and the last of these points must be horizontal. If the reaction rate function $F(\theta^*)$ is convex-concave, more precisely, if $F'(\theta^*)$ is a positive function of θ^* with exactly one maximum, where $F''(\theta^*)$ has its unique nondegenerate zero, then there are at most two horizontal points. This includes the case of an Arrhenius law for the reaction rate.*

We conclude this subsection with a proof of the second part of Proposition 3.2. Thus we assume that F is convex-concave and that we have a solution curve with horizontal points. We recall the asymptotic behaviour (3.8). The first horizontal point must occur at some $\theta^* = \theta_1$, where, in view of (3.13), $(\theta^+)' > 0$ and μ'' and F'' have the same sign. Obviously the possibility that $\mu'' < 0$ in $\theta^* = \theta_1$ is excluded. For the last horizontal point, which occurs at some $\theta^* = \hat{\theta}_1$, the possibility that $\mu'' > 0$ in $\theta^* = \hat{\theta}_1$ is excluded. Clearly $\theta_1 \le \hat{\theta}_1$. Equality would mean that there is only one horizontal (inflection) point, but that the solution curve has no real turning points. This is a border line case between a solution curve without horizontal (and thus also without vertical points) and a solution curve with more than one horizontal point.

Let us continue with this latter possibility in which, by similar reasoning again, we must have $\theta_1 < \hat{\theta}_1$ and $\mu'' \ge 0$ in $\theta^* = \theta_1$, while $\mu'' \le 0$ in $\theta^* = \hat{\theta}_1$. Since μ'' and F'' have the same sign in horizontal points by (3.13), it follows that $F''(\hat{\theta}_1) \le 0 \le F''(\theta_1)$. Hence the (unique) zero θ_0 of F'' satisfies $\theta_0 \in [\theta_1, \hat{\theta}_1]$. We claim that θ_1 and $\hat{\theta}_1$ are the only horizontal points. By the definition of θ_1 and $\hat{\theta}_1$, any other horizontal points must lie between θ_1 and $\hat{\theta}_1$. We argue by contradiction from the assumption that there are horizontal points θ_2 and $\hat{\theta}_2$ with $\theta_1 < \theta_2 \le \hat{\theta}_2 < \hat{\theta}_1$ with $\mu''(\theta_2) \le 0 \le \mu''(\hat{\theta}_2)$. This would imply $F''(\theta_2) \le 0 \le F''(\hat{\theta}_2)$. Clearly, the assumptions on F then only allow equalities. The remaining possibility is thus that $\theta_2 = \hat{\theta}_2$ is an inflection point, and $\mu(\theta_1) < \mu(\theta_2) < \mu(\hat{\theta}_1)$ are the only horizontal points. However, $F'''(\theta_2) < 0$ and a short calculation reveals that $\mu'''(\theta_2)$ has the same

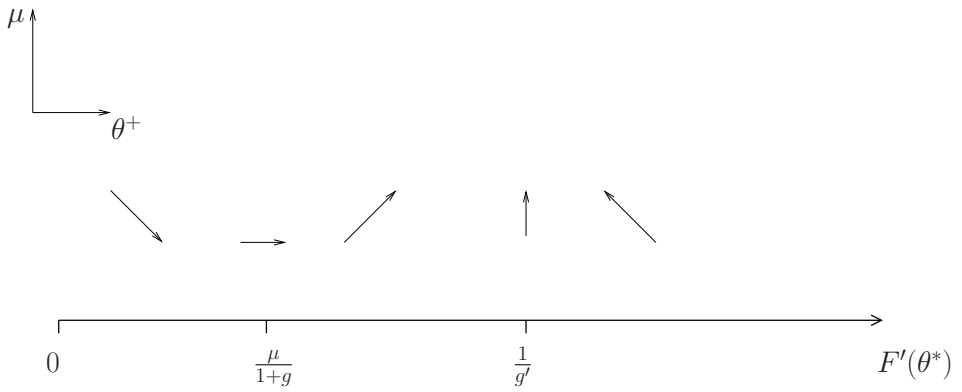

Figure 4: Dependence on $F'(\theta^*)$ of the tangent vector in the bifurcation diagram.

sign as $F'''(\theta_2)$ in such an inflection point, hence this also leads to a contradiction. This completes the proof.

3.2 Turning points, a different perspective

If the solution curve (3.7) has horizontal turning points, it may or may not have vertical turning points. In order to explain this we take a slightly different perspective and observe that the reaction rate function F only appears at the very end of our calculations. We can in fact consider it as a (function-valued) parameter of the travelling wave problem. Our calculations show that with the reaction rate unspecified, every choice of $\alpha, \chi, \mu, \theta^-, \theta^+$ determines a unique travelling wave with θ^* specified by (2.28). For any choice of F with $F(\theta^*)$ satisfying (3.2), this travelling wave is a travelling wave solution of the full problem. Clearly, by modifying F we can make the bifurcation curve move in any direction we want starting from this particular value of θ^*, subject only to the restrictions imposed by (3.12,3.13). This information is summarised in Figure 4, where the direction in which (3.7) moves is sketched for various ranges of $F'(\theta^*)$. Note that vertical turning points are only possible if $g'(\mu) > 0$. In that case, if $F(\theta^*)$ is sufficiently steep as a function of θ^*, the bifurcation diagram will have at least one S-shaped part, as depicted in Figure 2.

Restricting to Arrhenius reaction rates (1.7) and given a travelling wave as above with $g'(\mu) > 0$, we can easily choose ε and θ_c to ensure (3.2) holds. When θ_c and ε are varied under this constraint, which reads

$$\varepsilon \log F(\theta^*) = \frac{1}{\theta_c} - \frac{1}{\theta^*},$$

we have that $F'(\theta^*)$ is given by (3.9). We can make ε as small and thus $F'(\theta^*)$ as large as we want. It follows that vertical turning points indeed occur.

Note though that the range along which $F'(\theta^*)$ may be varied is bounded by $(-\log F(\theta^*))F(\theta^*)/\theta^*$ from below if $F(\theta^*) < 1$. See also [8], where $\theta_c = 2\theta^+ - \theta_-$ is taken in a suitable high activation limit, with θ^+ fixed.

4 Numerical computations for the bifurcation diagram

In this section we use the formulas from the previous sections to compute numerically the bifurcation diagrams in the (θ^+, μ)-plane. The solution curve is parameterised by θ^*. For the numerical calculations we use the AUTO software package [5]. In particular, we implement the algebraic system that consists of (3.1), (3.2) and (2.16) for the unknowns θ^*, a_3, μ and θ^+. We use the Arrhenius law (1.7) for the reaction rate and recall it here:

$$F(\theta^*) = \exp\left(\frac{1}{\varepsilon}\left(\frac{1}{\theta_c} - \frac{1}{\theta^*}\right)\right).$$

In the previous section we discussed the turning points and all possible directions of the curve in the bifurcation diagram, see Figure 4. We also explained how the turning points depend on $F'(\theta^*)$, considered as independent parameter. In this section we relate the analytical results to the obtained figures. Our approach to compute the bifurcation diagram numerically is to fix a point in the (θ^+, μ)-plane and then vary $F'(\theta^*)$, by varying ε and θ_c, to scan through the possible directions of the diagram, see Figures 2 and 6. We start from a solution $(\theta^+, \mu, \theta^*)$ for which the corresponding $g'(\mu) > 0$. We know from Proposition 3.2 that the parameterised solution curve continues down to $\theta^* = \theta^-$ with $\mu \to \infty$ and $\theta^+ \to \theta^-$ and continues up to $\theta^* \to \infty$, with $\mu \to 0$ and $\theta^+ \to \infty$.

It is hard to give plots which show global and local details simultaneously. One should keep in mind that the model is derived based on the assumption that reaction rate is a steep function. Therefore both limits, $\theta^* \to \theta^-$ and $\theta^* \to \infty$ are less physical. Indeed the first corresponds to an almost flat profile with very large speed. Clearly a flat profile is a trivial travelling wave for which the concept of speed has no meaning. Solutions with large θ^* are less relevant, requiring very large y^-. In the plots we give global pictures and then zoom in at the physically relevant range, where the interesting phenomena occur. A logarithmic scale is used to produce the global pictures and a normal scale for the zoomed-in pictures.

A general feature of our numerical results is that only for small ε we find turning points. Moreover, vertical turning points require tuning the radiative parameters. In Figure 5 we plot a solution diagram for various values of the ε (and their corresponding θ_c). For $\varepsilon = 0.7$ and $\varepsilon = 0.3$, the solution diagrams, the dashed-dotted and dotted lines, show monotonically descending curves. Taking a larger activation energy, i.e. smaller ε, the solution diagram has two horizontal turning points and no vertical one, as described by the smaller-dashed and the bigger-dashed lines for, respectively, $\varepsilon = 0.2$ and $\varepsilon = 0.1$. For the solution diagram to have a vertical turning point a much larger activation energy (smaller ε) should be taken. Taking $\varepsilon = 0.04$, the solid line (solution curve) in Figure (5) has an S-shaped part (see also Figure 6). One can see that this curve has two horizontal turning points and two vertical turning points. Notice that the first and the last turning points are horizontal, which agrees with the discussion in section 3.

In Figure (7) we compare the solution diagram for the values of $\alpha = 0.1, \alpha = 0.05$ and $\alpha = 0.02$, starting from the final curve in Figure 5 ($\varepsilon = 0.04$). Zooming in, in the same figure, shows that as the opacity α decreases (the medium becoming more transparent), the flame speed μ increases in the

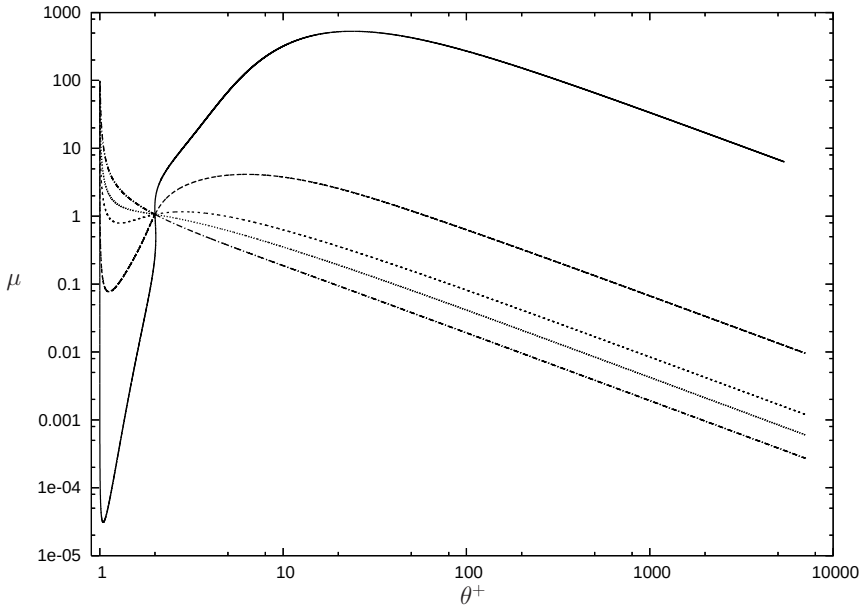

Figure 5: The solution diagram in the (θ^+,μ)-plane parameterised by θ^*: $\varepsilon = 0.04, \theta_c = 2.39$ (solid), $\epsilon = 0.1, \theta_c = 2.37$ (bigger dashed), $\varepsilon = 0.2, \theta_c = 2.34$ (smaller dashed), $\varepsilon = 0.3, \theta_c = 2.3$ (dotted) and $\varepsilon = 0.7, \theta_c = 2.1$ (dashed-dotted). Radiative parameters: $\chi = 1$, $\alpha = 0.1$

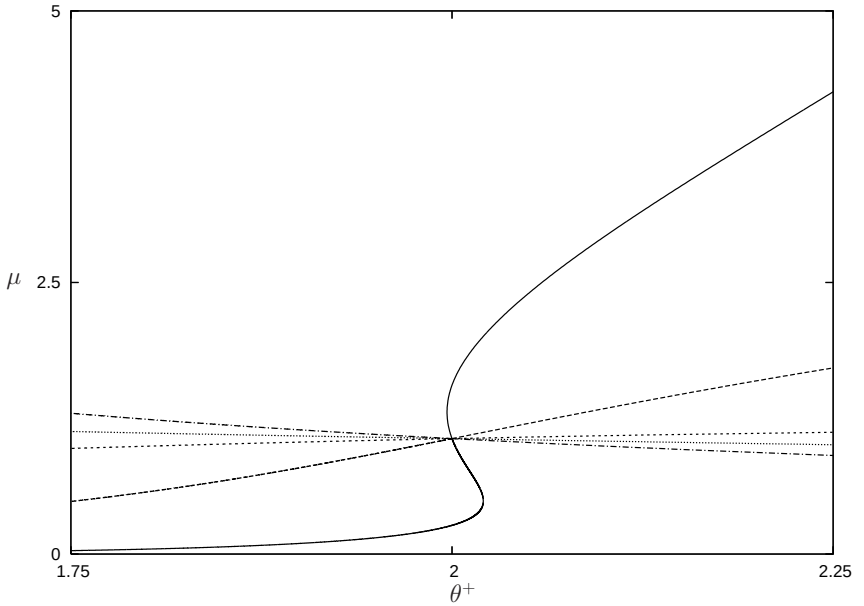

Figure 6: Zooming in for Figure 5

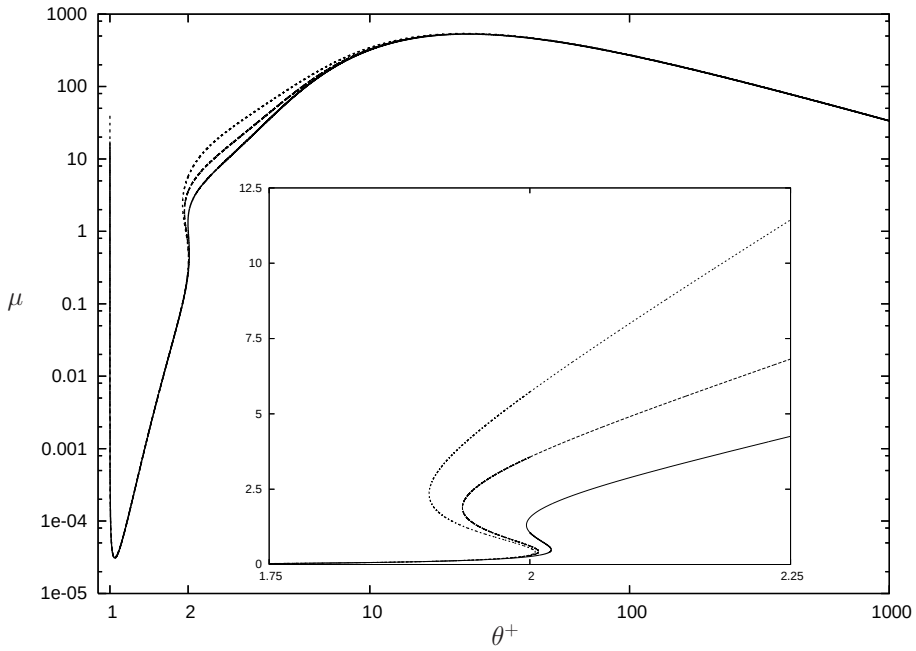

Figure 7: The solution diagram in the (θ^+,μ)-plane parameterised by θ^*, for $\theta_c = 2.39$, $\varepsilon = 0.04$ and $\chi = 1$, with $\alpha = 0.1$ (solid), $\alpha = 0.05$ (dashed), $\alpha = 0.02$ (dotted). The picture inside (zooming in) shows the S-shaped part.

upper part of the $S-$shaped curve (after the second turning point) while it decreases in the middle part of the curve (between the two vertical turning points).

5 Limit cases

In this section we examine limit cases in which we can explicitly determine the limit solution curve (3.7). We briefly discuss three cases:

- transparent limit: $\alpha \to 0$ and $\beta > 0$ fixed;
- radiation dominated limit: $\beta \to \infty$ and $\alpha > 0$ fixed;
- transparent and strongly radiation dominated limit: $\alpha \to 0$ and $\alpha\beta > 0$ fixed;

all with a fixed reaction rate $F(\theta^*)$. These limit cases were also considered in [2] and motivated earlier in [3, 6]. In [2] though, only fixed values of θ^+ were considered. Here we will consider the limit for the bifurcation diagram as a whole.

In view of the different physical nature of the parameters α and β it is natural to consider limit cases for α with $\beta > 0$ fixed and vice versa. Two of these four cases were nontrivial in [2] and therefore

included in our exposition. The third limit case above is of interest because it reduces the system while still producing nontrivial bifurcation diagrams, see [1].

A fourth limit case is more difficult, namely the transparent and weakly radiation dominated limit: $\alpha\beta \to 0$ and $\beta \to \infty$. Here we fix θ^+, take F given by (1.7) and couple ε to the radiative parameters α and/or β, depending on the dominant balance. Choosing $\theta_c = 2\theta^+ - \theta^-$, i.e. taking the upper limit on the flame temperature as characteristic temperature, we quickly recover the speed law obtained in [8] by a formal and highly nontrivial multi-scale analysis.

Before examining the limit cases we recall the solution diagram (3.7) and the temperature profile in the adiabatic case, i.e. $\beta = 0$.

5.1 Adiabatic case: $\beta = 0$

The adiabatic case is the model without radiative effects. This is equivalent to setting $\beta = 0$ in (2.3) whence $Q = 0$ in (2.2).

We recall that the cubic polynomial $P(a) = (a^2 - 3\alpha^2)(a - \mu) - \alpha\beta a$ in (2.16) has three roots $a_1 > a_2 > 0 > a_3$. For $\beta = 0$ we have

$$a_1 = \mu; \quad a_{2,3} = \pm\sqrt{3}\alpha,$$

whence (2.29) implies that $g(\mu) = 0$, the adiabatic bifurcation diagram is given by

$$\mu(\theta^+ - \theta^-) = F(\theta^+), \qquad \theta^* = \theta^+.$$

The adiabatic temperature profile is given by

$$\theta(x) = \theta^- + (\theta^+ - \theta^-)\min(\exp(\mu x), 1). \tag{5.1}$$

5.2 Transparent limit: $\alpha \to 0$ and $\beta > 0$ fixed

For $\alpha \to 0$ it is easily seen that

$$a_1 - \mu \sim \frac{\alpha\beta}{\mu}; \quad a_{2,3} \sim \frac{-\beta \pm \sqrt{\beta^2 + 12\mu^2}}{2\mu}\alpha$$

whence (2.29) implies that

$$g(\mu) \sim \frac{1}{\sqrt{1 + \frac{12\mu^2}{\beta^2}}}.$$

In view of (3.1,3.2) the limit curve in the bifurcation diagram is given by

$$\mu(\theta^+ - \theta^-) = F(\theta^*), \quad \theta^* = \theta^+ + \frac{\theta^+ - \theta^-}{\sqrt{1 + \frac{12\mu^2}{\beta^2}}}. \tag{5.2}$$

Since θ^* decreases with $\mu > 0$, we see immediately that for any combination of the parameters there is exactly one μ which solves (5.2). The limit temperature profile is given by

$$\theta(x) = \theta^- + (\theta^+ - \theta^-)\min(\exp(\mu x), 1) + \frac{\theta^+ - \theta^-}{\sqrt{1 + \frac{12\mu^2}{\beta^2}}}, \tag{5.3}$$

a uniformly lifted adiabatic profile. These results agree with [2, Proposition 3.2].

In this limit the function $g(\mu)$ is decreasing and vertical turning points cannot occur, in view of (3.10). Formula (5.3) again exhibits the range $[\theta^-, 2\theta^+ - \theta^-]$ for the admissible flame temperature θ^*.

5.3 Large Boltzmann number: $\beta \to \infty$ and $\alpha > 0$ fixed

As $\beta \to \infty$, the roots of P satisfy

$$a_{1,3} \sim \pm\sqrt{\alpha\beta}; \quad a_2 \sim \frac{3\mu\alpha}{\beta},$$

whence (2.29) implies that when $\beta \to \infty$, $g(\mu) \to 0$, so, in term of the bifurcation diagram, we recover the adiabatic case,

$$\mu(\theta^+ - \theta^-) = F(\theta^+), \quad \theta^* \to \theta^+.$$

Note however that $\theta(x)$ converges to θ^+ uniformly on bounded intervals, while the jump $[\theta']$ remains positive. In [2, Proposition 3.4] an inner region argument was needed to obtain this description. Here it follows directly from (2.25) and (2.26) which, to leading order gives

$$\theta(x) \sim \theta^+ + (\theta^+ - \theta^-)\frac{\mu}{2\sqrt{\alpha\beta}} e^{-\sqrt{\alpha\beta}|x|}.$$

5.4 Transparent limit combined with large Boltzmann numbers: $\alpha \to 0$ and $\chi = \alpha\beta$ constant

We have

$$a_{1,3} \sim \frac{\mu \pm \sqrt{\mu^2 + 4\chi}}{2}; \quad a_2 \sim \frac{3\mu\alpha^2}{\chi},$$

whence (2.29) implies that

$$g(\mu) \sim \frac{1}{\sqrt{1 + \frac{4\chi}{\mu^2}}},$$

so that the limit curve is given by

$$\mu(\theta^+ - \theta^-) = F(\theta^*), \quad \theta^* = \theta^+ + \frac{\theta^+ - \theta^-}{\sqrt{1 + \frac{4\chi}{\mu^2}}}. \tag{5.4}$$

Now, in the second expression, θ^* increases with $\mu > 0$ because in the limit $g'(\mu)$ is positive. This limit is complementary to the limit $\alpha \to 0$, β fixed, in which in the limit $g'(\mu)$ is negative. Since F is bounded, there is at least one solution μ. Generically there are an odd number of solutions. The limit temperature profile is given by

$$\theta(x) = \theta^+ + \frac{\theta^+ - \theta^-}{\sqrt{1 + \frac{4\chi}{\mu^2}}} \min\left\{ \exp\left(\frac{\mu - \sqrt{\mu^2 + 4\chi}}{2} x \right), \exp\left(\frac{\mu + \sqrt{\mu^2 + 4\chi}}{2} x \right) \right\}. \tag{5.5}$$

One can see that, in this limit the left boundary condition $\theta(-\infty) = \theta^-$ is lost (as in the limit $\beta \to \infty$, $\alpha > 0$). This is physically interpreted as that the preheating temperature is achieved at $x \to -\infty$, see [2] (and the references therein).

Note that as $\chi \to 0$, the flame temperature θ^* approaches $2\theta^+ - \theta^-$, the upper bound for the flame temperature, consistent with the result in [2, Proposition 3.5].

5.5 High flame temperature: $\alpha \to 0$, $\beta \to \infty$ and $\chi \to 0$

This limit is motivated by the previous subsection, where the flame temperature approaches its upper bound $2\theta^+ - \theta^-$ in the double limit $\alpha \to 0$ with $\chi > 0$ fixed followed by $\chi \to 0$. Note that $\alpha\beta \to 0$ and $\beta \to \infty$ imply that $\alpha \to 0$.

In the combined limit $\chi = \alpha\beta \to 0$, $\beta \to \infty$ we have

$$a_1 - \mu \sim \frac{\chi}{\mu}\left(1 - \frac{\chi}{\mu^2} + \cdots\right); \quad a_2 \sim \frac{3\mu\chi}{\beta^2}; \quad a_3 \sim \frac{\chi}{\mu}\left(-1 + \frac{\chi}{\mu^2} - \frac{3\mu^2}{\beta^2} + \cdots\right),$$

so that (2.29) implies that

$$g(\mu) \sim 1 - \frac{2\chi}{\mu^2} - \frac{6\mu^2}{\beta^2} + o(\chi) + o(\frac{1}{\beta^2}),$$

locally uniform in $0 < \mu < \infty$. Thus $g(\mu) \to 1$ from below.

Now (3.1,3.2), combined with the Arrhenius reaction rate (1.7), lead to

$$\varepsilon \log\left(\mu\left(\theta^+ - \theta^-\right)\right) = \frac{1}{\theta_c} - \frac{1}{\theta^*} \approx \frac{1}{\theta_c} - \frac{1}{2\theta_+ - \theta^-} - \frac{\theta^+ - \theta^-}{(2\theta^+ - \theta^-)^2}(1 - g(\mu)).$$

Provided we take

$$\theta_c = 2\theta_+ - \theta^-,$$

we arrive at

$$\varepsilon \log\left(\mu\left(\theta^+ - \theta^-\right)\right) = -\frac{\theta^+ - \theta^-}{(2\theta^+ - \theta^-)^2}\left(\frac{2\chi}{\mu^2} + \frac{6\mu^2}{\beta^2} + o(\chi) + o(\frac{1}{\beta^2})\right). \tag{5.6}$$

The limit $\varepsilon \to 0$ gives a nontrivial limit if ε is taken to balance the largest of χ and $1/\beta^2$ (or both). The double balance occurs with the scaling, see [8],

$$\alpha = \alpha_0\varepsilon^{3/2} \qquad \beta = \beta_0\varepsilon^{-1/2} \qquad \chi = \chi_0\varepsilon, \tag{5.7}$$

In this case, the relation for the asymptotic speed μ_0 reads

$$\log\left(\mu_0\left(\theta^+ - \theta^-\right)\right) = -\frac{\theta^+ - \theta^-}{(2\theta^+ - \theta^-)^2}\left(\frac{2\chi_0}{\mu_0^2} + \frac{6\mu_0^2}{\beta_0^2}\right), \tag{5.8}$$

consistent with [8, Equation (46)]

6 Conclusion

We have presented a 'linear' radiative combustion model for general Lewis number and radiative parameters α and β. We have extensively studied the travelling waves for this model. We proved that, dropping the reaction rate, there exists a travelling wave profile for every value of the flame speed $\mu > 0$. Taking the reaction rate into account, we have shown that in the (θ^+, μ) plane travelling waves

are given by a single smooth curve which is parameterised by the flame temperature θ^*. This curve may have turning points and exhibit S-shaped parts, which motivates the further study of stability of these solutions. The bifurcation diagram does not depend on the Lewis number, see also [1]. Varying Lewis we expect the stability properties of the solutions to change. Finally, we determined the solution curve for physically interesting asymptotic regimes of the radiative parameters.

References

[1] Olivier Baconneau, Jan Bouwe van den Berg, Claude-Michel Brauner, and Josephus Hulshof. Multiplicity and stability of travelling wave solutions in a free boundary combustion-radiation problem. *European J. Appl. Math.*, 15(1):79–102, 2004.

[2] C.-M. Brauner, J. Hulshof, and J.-F. Ripoll. Existence of travelling wave solutions in a combustion-radiation model. *Discrete Contin. Dyn. Syst. Ser. B*, 1(2):193–208, 2001.

[3] J Buckmaster and T. L Jackson. The effects of radiation on the thermal-diffuse stability boundaries of premixed flames. *Combust. Sci and Tech*, 103:299–313, 1994.

[4] J. Buckmaster, G Joulin, and P. Ronney. The effect of the radiation on flame balls at zero gravity. *Combust and Flame*, 79:381–392, 1990.

[5] E.J. Doedel, A.R. Champneys, T.F. Fairgrieve, B. Kuznetsov, Y.A.and Sandstede, and X. Wang. Continuation and bifurcation software for ordinary differential equations (with homcont). *Available by anonymous ftp from ftp.cs.concordia.ca, directory pub/doedel/auto.*, AUTO97, 1997.

[6] G Joulin and B. Deshaies. On radiation-affected flame propagation in gasueos mixtures seeded with inert particles. *Combust. Sci. and Tech*, 79:299–315, 1986.

[7] A A Shah, R W Thatcher, and J W Dold. Stability of a spherical flame ball in a porous medium. *Combust. Theory Modelling*, 4:511–534, 2000.

[8] Jan Bouwe van den Berg, Claude-Michel Brauner, Josephus Hulshof, and Alessandra Lunardi. The speed law for highly radiative flames in a gaseous mixture with large activation energy. *SIAM J. Appl. Math.*, 66(2):408–432 (electronic), 2005.

[9] Forman A. Williams. *Combusion Theory*. Perseus Books Publishing, second edition edition, 1985.